ACS APPLIED MATERIALS & INTERFACES

Research Article

www.acsami.org

Field Emission in Vertically Aligned ZnO/Si-Nanopillars with Ultra Low Turn-On Field

Yuan-Ming Chang,*[,†] Mao-Chen Liu,[‡] Pin-Hsu Kao,[§] Chih-Ming Lin,[⊥] Hsin-Yi Lee,[#,∥] and Jenh-Yih Juang*[,†]

[†]Department of Electrophysics and [∥]Department of Materials Science and Engineering, National Chiao Tung University, Hsinchu 300, Taiwan

[‡]National Nano Device Laboratory, Tainan 741, Taiwan

[§]Center for Measurement Standards, Industrial Technology Research Institute, Hsinchu 300, Taiwan

[⊥]Department of Applied Science, National Hsinchu University of Education, Hsinchu 300, Taiwan

[#]National Synchrotron Radiation Research Center, Hsinchu 300, Taiwan

ABSTRACT: An effective method of fabricating vertically aligned silicon nanopillars (Si-NPs) was realized by using the self-assembled silver (Ag) nanodots as natural metal-nanomask during dry etching process. The obtained Si-NPs were preferentially aligned along the *c*-axis direction. Ultrathin ZnO films (~9 nm) were subsequently deposited on the Si-NPs by atomic layer deposition (ALD) to enhance the field emission property. The average diameter of the ZnO/Si-NPs is in the order of tens of nanometers, which enables efficient field emission and gives rise to marked improvement in the field enhancement factor, β. The turn-on field defined by the 10 μA/cm^2 current density criterion is ~0.74 V/μm with an estimated $\beta \approx 1.33\times10^4$. The low turn-on field and marked enhancement in β were attributed to the small radius of curvature, high aspect ratio, and perhaps more importantly, proper density distribution of the ZnO/Si-NPs.

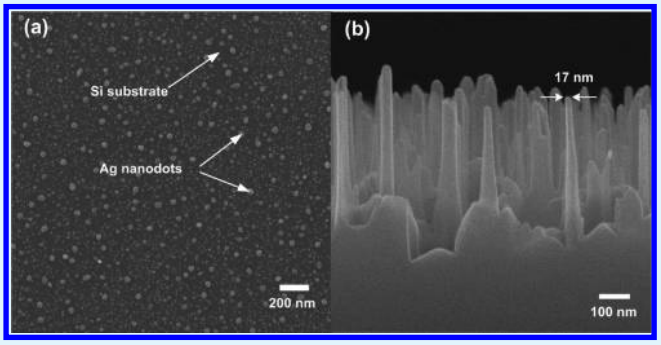

KEYWORDS: *filed emission, ZnO, silicon nanopillars, atomic layer deposition*

INTRODUCTION

Due to a plethora of attractive properties and potential applications, tremendous efforts have been put forth in manufacturing the one-dimensional (1D) semiconductor nanostructures and using them to fabricate high-performance electronic devices.[1−5] However, because of the susceptibility of forming native oxide even at ambient conditions, using the 1D Si nanostructures for field emitters has not been considered as advantageous as those devices mentioned above. One of the primary reasons is that, in this case, most of the field-emission electrons will be trapped in the interface between Si and the native oxide layer. To overcome the important issue of electron trapping, increasing the driving field appears to be inevitable to liberate electrons from Si emitters. This approach, unfortunately, will consume considerably more energy and, thus, is undesirable. To fully realize the application potential of the 1D Si nanostructures, especially in the area of field emission, alternative ways of lowering the turn-on field and at the same time increasing the enhancement factor of the Si nanoemitters are required. In this study, we report an efficient method of fabricating ZnO/Si-nanopillar (ZnO/Si-NP) heterostructures, which exhibited very low threshold field and relatively high field enhancement factor.

In the present study, self-assembled silver (Ag) nanodots produced by single-step sputtering were used as the metal-mask for the subsequent dry etching process carried out to fabricate the 1D Si-NPs. Briefly, the obtained Si-NPs exhibited the following three important structural characteristics: (1) small radius of curvature (typically around 10 nm) at the tip of the pillars; (2) the Si-NPs are having a high aspect ratio of ~10; and (3) the ratio between the pillar spacing and height (R/H) is close to the optimal value such that the field screen effect is minimized. High-resolution transmission electron microscopy (HRTEM) reveals that the Si-NPs obtained by the present process remain single crystalline. Because the Si-NPs were manufactured by using the self-assembled Ag nanodots array created by single-step sputtering as the natural metal-nanomask and the dry etching process was performed without any lithography process involved, thus the fabrication cost can be reduced significantly.

Moreover, to resolve the problem of the native SiO_x formed at the surface of the Si-NPs and, hence, to enhance the their performance in field emission, a 9-nm-thick ZnO film was

Received: November 28, 2011
Accepted: January 30, 2012
Published: January 30, 2012

deposited at 200 °C on the Si-NPs by atomic layer deposition (ALD) method. It is noted that previously direct growth of ZnO films on Si substrates has been suffering from severe degradation of crystalline quality due to the fact that SiO_x is chemically more stable than ZnO and the ZnO films were virtually grown on SiO_x layer instead of the better crystalline Si substrate. Nevertheless, the ZnO layers obtained in the present study are all having decent crystalline quality albeit they are mostly polycrystalline. The HRTEM analyses indicate that, indeed, no apparent SiO_x layer is immediately discernible. This somewhat surprising feature presumably is resulted from the low growth temperature practiced in the present ALD process. Finally, due to proper pitch between the nearest Si-NPs, the present ZnO/Si-NPs exhibit an unprecedentedly low threshold field and a relatively large field enhancement factor for electron emission.

MATERIALS AND METHODS

The Ag nanodots grown on Si substrates were obtained by rf-sputtering from an Ag target (Eastern Sharp EPS01) for 5 seconds with an input power of 150 W in 25 sccm argon (Ar) gas atmosphere. The Si-NPs array was obtained by subsequent dry etching performed in a metal etcher system (Canon 4100). Prior to etching, the chamber was evacuated to a base pressure of 3×10^{-5} Torr while the system temperature was kept at 60 °C. After loading the prepared Ag nanodots covered Si substrate, Cl_2 gas of 90 sccm and N_2 gas of 10 sccm were introduced. The system was operated with a fixed input power of 1900 W and the etching time was 5 minutes. The Si substrate with Si-NPs was etched using a standard buffered oxide etch (BOE) for 5 minutes to ensure complete removal of the native oxides prior to carrying out the ZnO deposition. Ultrathin ZnO films were deposited onto the nanopillars-covered Si substrate at 200 °C by atomic layer deposition (ALD). For ALD process, briefly, the pulse durations of water and diethylzinc (DEZn) were 100 ms and 50 ms, respectively. The purge and pumping periods were 15 s and N_2 was used as the purge gas with the pressure being set to 5×10^{-2} Torr. The above deposition procedures were used for depositing ultrathin ZnO films on the surface of Si-NPs for 30 ALD cycles.

A field-emission scanning electron microscopy (FESEM, JEOL JSM-6700F) was used to examine the morphology of the Si-NPs. For cross-sectional transmission electron microscopy (XTEM) investigations specimens cut from the stacked wafers of ZnO/Si-NPs were mechanical polished down to 20−30 μm-thick, followed by Ar ion milling to finally obtain electron transparency. TEM (JEOL JEM-2010F) with an operating voltage of 200 kV was employed to observe the ZnO/Si-NPs heterostructures.

The photoluminescence (PL) measurements were carried out at room temperature using a He−Cd laser (325 nm, IK3252R-E, Kimmon) for excitation and a CCD (80 K, Spec-10, Princeton Instruments) with a monochromator (0.5 m, SP-2558A, Acton) for detection. Moreover, the samples were loaded into a vacuum chamber to measure the field-emission current. The phosphor (P_{22}), which was applied in the cathode-ray tube displays, was deposited on a transparent conductive material (indium−tin-oxide), to serve as the anode electrode in the vacuum system and the cathode voltage was applied to the Si substrates. The schematic diagram for the setup of the field-emission measurements is shown in Figure 1. The distance between the sample and electrode is 350 μm and the chamber pressure being kept at 2×10^{-6} Torr during all the field-emission measurements.

RESULTS AND DISCUSSION

Figure 2a reveals the SEM image showing the typical morphology and distribution of the Ag nanodots, which were obtained with a sputtering time of 5 s. The density of the Ag nanodots (with diameter >30 nm) is estimated to be around 6.4×10^9 cm^{-2}. Furthermore, it is evident from the SEM image

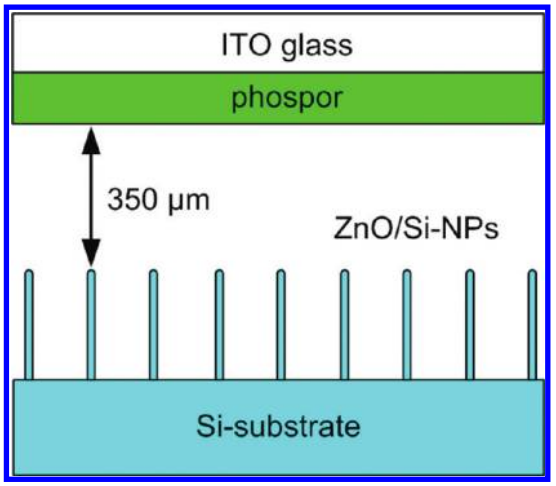

Figure 1. Schematic diagram of the field-emission measurement.

that, although the size of the isolated islands does display a distributed characteristic, there appears no apparent coalescence between Ag islands, presumably due to the very short sputtering time of only 5 s. The characteristic is believed to arise from the film growth mechanism inherent to the current system and can be understood as follows. Because the surface energies for Ag and SiO_2 are about 923 and 200−260 ergs/cm^2, respectively,[6,7] one expects that the deposited Ag layer would follow the Volmer-Weber growth mode and grow into island-like morphology during the processes of sputtering. The nucleation and growth of the individual islands, thus, is prevailed predominantly by surface diffusion of the impingement of condensate monomers, rather than the thermal-induced dewetting and subsequent agglomeration of an existing thin layer frequently observed in processes involving post-deposition annealing.[8−10]

Figure 2b displays the Si-NPs obtained by performing the dry etching process for 5 minutes directly on the Si substrate partially covered with the Ag nanodots shown in Figure 2a. The Si-NPs obtained under this condition are having an average height of 350−450 nm with an average inter-pillar spacing of 150−250 nm and an aspect ratio of ∼10. Additionally, it is noted that the diameter of the Si-NPs' tip can be as small as only ∼17 nm, as marked on one of the Si-NPs shown in Figure 2b. Obviously, the Ag nanodots have played an important role as effective metal-nanomask during the early stage of dry etching performed on the Si substrate. They provided effective protection to prevent the areas underneath from ion bombardment during dry etching process while significant anisotropic etching was prevailing on the exposed areas of the Si substrate. We found that within an etching time of about 5 minutes the Ag nanodots appeared to vanish completely. As displayed in Figure 2b, the Si-NPs are aligned vertically along the [001] crystallographic orientation. The spacing between the Si-NPs is about 150−250 nm, which in fact, agrees very well with the distance between the Ag nanodots with diameter larger than 30 nm (as shown in Figure 2a), indicating the effectiveness of using them as etching masks. It is also worthwhile to note that, unlike observed in many other 1-D nanostructures (like carbon nanotubes) where the proximity of individual tips has resulted in significant field screening effects,[11] the current Si-NPs appears to have a very favorite ratio between the inter-pillar spacing and the pillar height (∼1/2) for field emission.[12,13] However, as will be shown below, the pristine Si-NPs do not

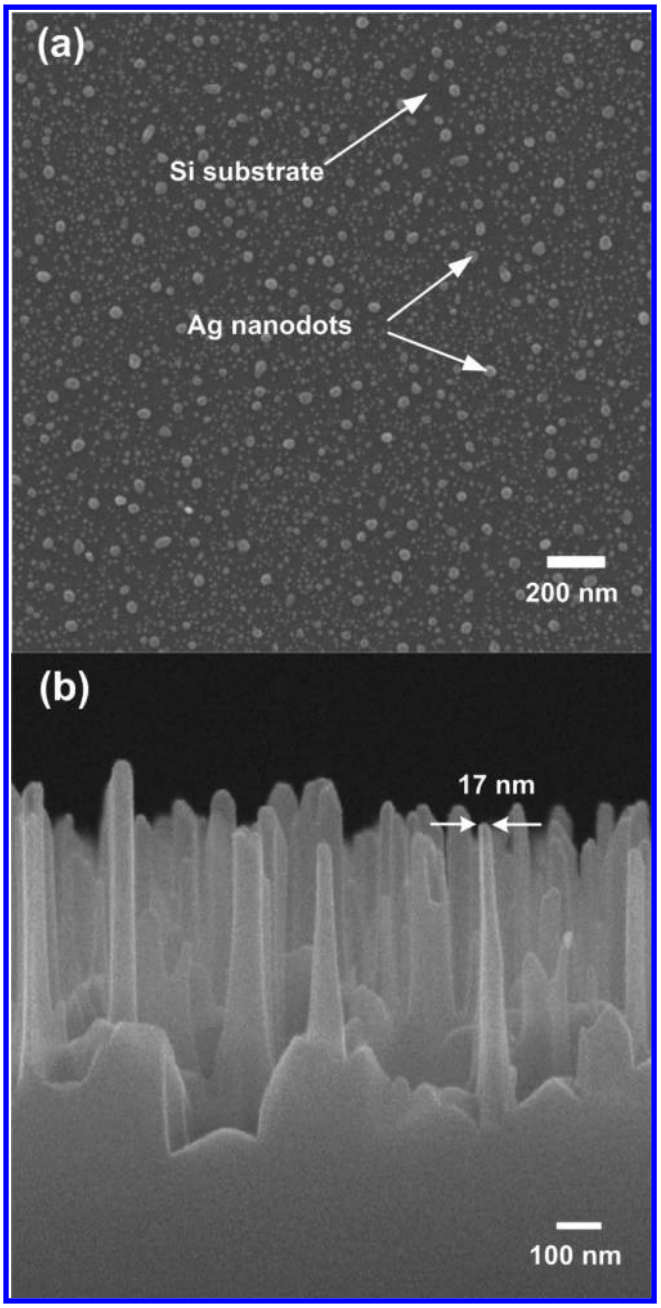

Figure 2. SEM images of (a) Ag nanodots array and (b) Si-NPs array.

exhibit practically feasible field emission properties, presumably because of the formation of native silicon oxide and/or intrinsic electronic structure of silicon.

To harvest the potentially favorable field-emission implied by the unique morphological features of the present Si-NPs, we intentionally deposited an ultrathin layer of ZnO (~9 nm) on the Si-NPs at 200 °C by ALD. The purpose was to replace the insulating native SiO_x surface layer with potentially conductive oxide which is presumably immune to oxidation while keeping the favorable geometric morphology for field emission. The grazing incidence XRD results (not shown here) indicate that the deposited ZnO layer is of polycrystalline characteristic. This is further confirmed by the detailed structural information obtained from TEM examinations. Figure 3a displays the TEM image of some of the Si-NPs coated with a layer of 9 nm-thick ZnO film. It is evident that the deposition of the ZnO films

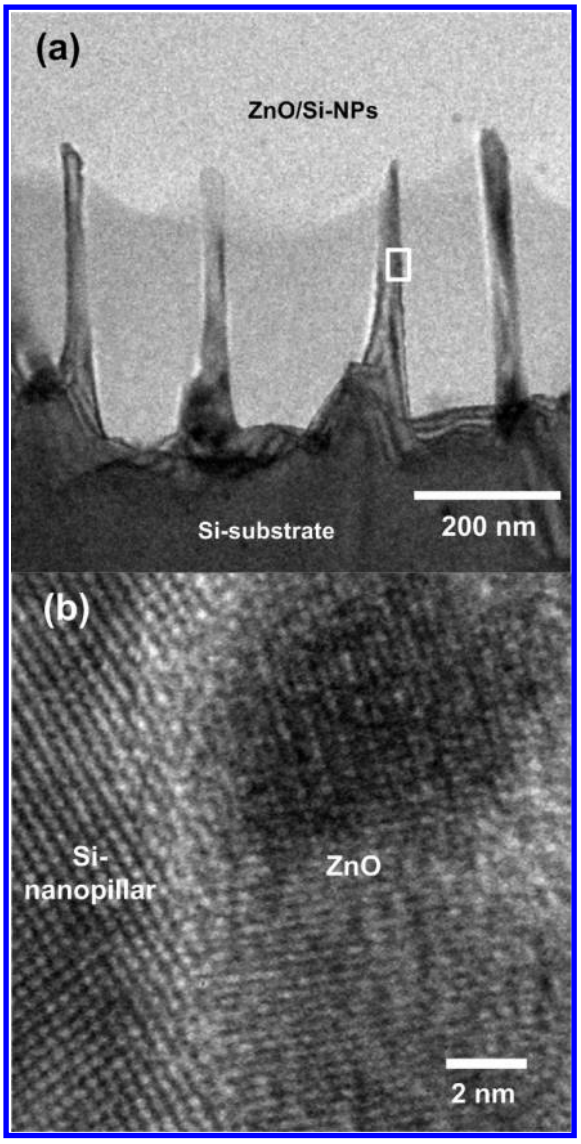

Figure 3. Structural analysis of the (9 nm) ZnO/Si-NPs heterostructure. (a) TEM image; and (b) the HRTEM of the area marked by the rectangle indicated in a.

does not result in noticeable changes on the morphological features of the original Si-NPs. Moreover, as displayed in the HRTEM image shown in Figure 3b for the area marked by the small square shown in Figure 3a, there are several features about the interface of the ZnO/Si-NPs to be noted.

Firstly, a layer of 9-nm-thick polycrystalline ZnO film with reasonable crystalline quality is uniformly deposited on the Si-NPs. Secondly, the single crystalline characteristics of the Si-NPs is essentially intact up to the very top surface layer, albeit being subjected etching processes and subsequent ALD at 200 °C. Thirdly, although there is trace suggesting the existence of a few atomic layer of SiO_x, the interface between the 9-nm-thick ZnO layer and Si-NPs appears to be fairly sharp. It is indicative that the deposition of the ZnO layer has effectively suppressed the formation of insulating SiO_x and hence may account for the improvement of field-emission effects to be discussed below.

Figure 4 shows the typical room temperature PL spectra obtained for the ZnO/Si-NPs. It can be observed from the spectra that the ZnO/Si-NP heterostructures exhibit a strong UV emission (3.26 eV) with a full-width-at-the-half-maximum

dx.doi.org/10.1021/am201667m | ACS Appl. Mater. Interfaces 2012, 4, 1411–1416

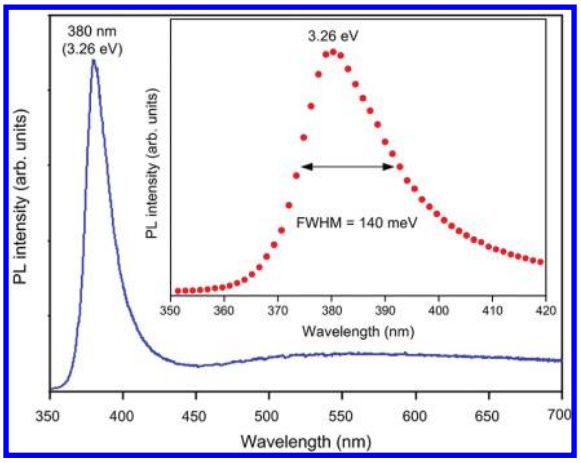

Figure 4. Room-temperature PL emission spectrum, showing a strong emission at 380 nm (3.26 eV).

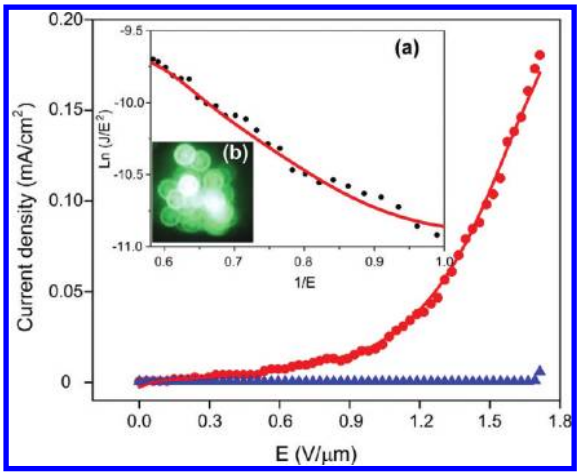

Figure 5. Field-emission $J-E$ curve from the Si-NPs (blue triangles) and ZnO/Si-NPs heterostructure array (red circles) at working distance of 350 μm over an effective emitting area of 1 × 1 cm^2. The Fowler–Nordheim plot [$\ln(J/E^2)$ vs $(1/E)$] is shown in inset a; inset b shows a green luminescence from a phosphor obtained at an electric filed of 1.7 V/μm.

(FWHM) approximately equal to 140 meV (see the inset of Figure 4) and a faded broad emission peak covering almost entire visible range. The former presumably is due to the recombination of free excitons through exciton–exciton collision processes and its relatively narrow FWHM is indicative of decent crystalline quality of the ZnO layer.[14−19] The latter, on the other hand, is generally conceived to result primarily from oxygen-vacancy related or Zn-interstitial defects residing near the surface of the ZnO layer.[20−25] More specifically, the green-yellow emission ubiquitously observed in most defective ZnO samples has been attributed to donor–acceptor pair transition involving oxygen vacancies.[26,27] Thus, for the present case, the dominant free-exciton UV-emission accompanied by a diminishingly weak broad visible emission peak seen in the PL spectrum indicates that the ZnO film is of high crystalline quality with relatively low concentration of oxygen vacancies. This is, in fact, quite consistent with that displayed in the HRTEM results shown in Figure 3b. A comparison of the PL characteristics displayed in the present ultrathin ZnO films to that of various ZnO nanostructures reported previously[28−30] also leads to similar conclusions. However, since the diameter of ZnO nanocrystals obtained in this work (see Figure 3b) is too large compared to the quantum dots obtained previously,[28,29] the size-confinement effect, thus, should not be considered. On the other hand, it is remarkable to note that excellent single-crystal-like PL properties can be still obtained albeit the significant lower growth temperature (200 °C) practiced in this study as compared to that used in the multistep buffering process reported previously.[30]

The next questions of interest will be how the coated ZnO thin layer affects the electronic properties of the Si-NPs and the associated field-emission performance for these nanopillar structures. Figure 5 shows the emission current density as a function of the applied electrical field ($J-E$ curves) for both the Si-NPs and ZnO/Si-NPs. The electric field was determined by dividing the applied voltage with the apparent cathode–anode separation. Thus, it is an averaged global field instead of local field at the tips of the nanostructures. Steady field emission was obtained by keeping the distance between the electrodes at 350 μm and the chamber pressure at 2 × 10^{-6} Torr during measurements. It is evident from Figure 5 that for the bare Si-NPs, only diminishingly small field-emission current was detected up the maximum applied field (~1.7 V/μm) of the current setup. This is presumably due to the existence of the native oxide layer which forms an insurmountable barrier for electron emission. On the other hand, for the ZnO/Si-NPs, the turn-on field, which was defined as the applied field required for drawing an emission current of 10 μA/cm^2, is as low as 0.74 V/μm. The turn-on field for the present ZnO/Si-NPs is much lower than most of the results obtained from various ZnO nanostructures reported previously, where the turn-on field defined by the same 10 μA/cm^2 criterion ranges from 3–15 V/μm.[31−36] It is noted that the emission current density reaches ~0.2 mA/cm^2 at the maximum bias field of our current setup (~1.7 V/μm), which also outperforms most of the ZnO nanostructures previously reported, where the current density reaches only 0–0.1 mA/cm^2 at an applied field of 1.7 V/μm.[31−36] Thus, it is indeed somewhat surprising that by merely depositing a 9-nm-thick ZnO film on the same Si nanostructures would lead to such drastic changes in the field-emission properties.

According to the classical Fowler–Nordheim (F–N) theory for field emission, the relation between the emission current density and the applied field can be expressed by the following F–N equation[36]

$$J = \frac{A\beta^2 E^2}{\phi} \exp\left(\frac{-B\phi^{3/2}}{\beta E}\right) \quad (1)$$

where J is the current density (A/m^2), E is the applied field (V/μm), ϕ is the work function (eV), β is the field enhancement factor, A and B are constants with $A = 1.56 \times 10^{-10}$ (A eV/V^2) and $B = 6.83 \times 10^3$ (V/μm eV$^{3/2}$), respectively. From eq 1, it is clear that the two primary parameters determining the emission characteristics of a particular structure are ϕ and β, which can be obtained experimentally by plotting $\ln(J/E^2)$ vs $1/E$, the so-called F–N plot. Inset (a) in Figure 5 shows the F–N plot for the ZnO/Si-NPs heterostructure, and inset (b) displays the light excited by the emitted electrons seen on the anode phosphor screen. By plotting $\ln(J/E^2)$ against $1/E$, a nearly straight line was obtained for the ZnO/Si-NPs. The quasi-linear behavior of the plot indicates that the field emission behavior of these heterostructures may have deviated from the F–N description slightly. It should be noted that the original F–N

theory was derived specifically for flat, metallic surfaces with work function on the order of 2−5 eV.[37] Thus, it might not be as exact when applied to other materials or to structures with different morphologies. It is nevertheless still an instructive practice to make some quantitative estimates using the F−N theory. The field enhancement factor β was calculated from the slope of the F−N plot[34]

$$\beta = (-2.97 \times 10^3)\phi^{3/2}/\text{slope} \quad (2)$$

By assuming the work function of ϕ = 5.3 eV for ZnO,[38] the β value of 1.33×10^4 was obtained. This β value is much larger than most field emitters reported and may need further discussions.

In order to check the validity of the obtained high β value in the present case, an independent estimate for the enhancement factor based on geometrical conditions of the emitter structure was performed. According to Zhao et al.,[39] the enhancement factor can be defined as

$$\beta \approx 1 + s(d/r) \quad (3)$$

Where s is the screening effect parameter, d and r are anode-to-cathode spacing and radius of curvature for the emitter, respectively. For the typical Si-NPs shown in Figures 2 and 3, the averaged r is taken to be 15 nm and d is 350 μm in our measurement setup. Thus, by assuming $s \approx 1$ (i.e., no field screening effect from the presence of neighboring emitters), one obtains $\beta \approx 2.33 \times 10^4$ from eq 3. It is interesting to observe that the β values respectively derived from eq 2 and eq 3 suggest a corresponding screening effect parameter of ~0.6, which, in fact, is consistent with the Utsumi's relative figure of merit for pillar-shape emitters.[40,41]

Finally, we noted that because of the slight differences in electron affinity χ and work function ϕ between Si and ZnO, there may also be some effects on the emission properties of the present ZnO/Si-NPs nanostructures. Taking χ_{Si} = 4.01 eV,[42] χ_{ZnO} = 4.35 eV,[43] ϕ_{Si} = 4.60-4.85 eV,[44] and ϕ_{ZnO} = 5.3 eV,[38] one would expect band edge discontinuity on order of 0.5 eV between the two semiconductors. Thus, further investigations are needed to clarify how this band edge discontinuity together with the inevitable charge accumulation/depletion at the interface would modify the actual work function of the resultant emitters, and hence modify the exact values of the estimated β values. Nevertheless, we believe that the ultralow turn-on field obtained from the combined effects of the unique morphological features and the surface modification resulted from coating a thin layer of ZnO film on the Si-NPs should have significant implications for various field emission-derived applications.

CONCLUSION

In summary, we have demonstrated an effective method for obtaining well-aligned Si-NPs with favorable morphological features for field emission by combining a single-step Ag sputtering with subsequent dry etching process. An ultralow threshold field of 0.74 V/μm and an extremely high field enhancement factor $\beta \approx 1.33 \times 10^4$ were obtained by depositing a 9 nm-thick of ZnO film on the Si-NPs. Comparing with most of the previous techniques employed to obtain similar 1D ZnO or Si nanostructures, the ZnO/Si-NPs demonstrated in the present study not only can be obtained by a simple and lithography-free process but also exhibit field-emission performances comparable to the best results reported. The present study, thus, has evidently provided significant potentials for various field-emission-derived applications.

AUTHOR INFORMATION

Corresponding Author

*Phone: +886-3-5712121, ext. 56116. Fax: +886-3-5725230. E-mail: ymchang7@gmail.com (Y.-M.C.); jyjuang@g2.nctu.edu.tw (J.-Y.J.).

Notes

The authors declare no competing financial interest.

ACKNOWLEDGMENTS

This work was partially supported by the National Science Council of Taiwan, under Grant NSC 100-2811-M-009-037. J.-Y.J. is supported in part by the National Science Council of Taiwan and the MOE-ATP program operated at NCTU. The authors would like to thank Prof. Hsi-Fu Shih, Prof. Ching-Liang Dai, and Jyun-Hao Wu for sputtering technical supports in Department of Mechanical Engineering, National Chung Hsing University, Taiwan. The authors also thank Dr. Yu-Hwa Shih, Dr. Jheng-Ming Huang (NCTU), Dr. Shang-Jui Chiu (NTHU), and Dr. Yen-Ting Liu (NCTU) for useful discussions.

REFERENCES

(1) Weng, W. Y.; Chang, S. J.; Hsu, C. L.; Hsueh, T. J. *ACS Appl. Mater. Interfaces* **2011**, *3*, 162−166.
(2) Das, S. N.; Kar, J. P.; Choi, J.-H.; Lee, T. I.; Moon, K.-J.; Myoung, J.-M. *J. Phys. Chem. C* **2010**, *114*, 1689−1693.
(3) Lupan, O.; Pauporté, T.; Viana, B.; Tiginyanu, I. M.; Ursaki, V. V.; Cortès, R. *ACS Appl. Mater. Interfaces* **2010**, *2*, 2083−2090.
(4) Suh, D.-I.; Lee, S.-Y.; Hyung, J.-H.; Kim, T.-H.; Lee, S.-K. *J. Phys. Chem. C* **2008**, *112*, 1276−1281.
(5) Quintana, M.; Edvinsson, T.; Hagfeldt, A.; Boschloo, G. *J. Phys. Chem. C* **2007**, *111*, 1035−1041.
(6) Bondi, A. *Chem. Rev.* **1953**, *52*, 417−458.
(7) Chang, Y.-M.; Shieh, J.; Juang, J.-Y. *J. Phys. Chem. C* **2011**, *115*, 8983−8987.
(8) Park, S.-J.; Lee, S.-W.; Lee, K.-J.; Lee, J. H.; Kim, K.-D.; Jeong, J.-H.; Choi, J.-H. *Nanoscale Res. Lett.* **2010**, *5*, 1570−1577.
(9) Lin, G.-R.; Chang, Y.-C.; Liu, E.-S.; Kuo, H.-C.; Lin, H.-S. *Appl. Phys. Lett.* **2007**, *90*, 181923−1-3.
(10) Lee, Y.; Koh, K.; Na, H.; Kim, K.; Kang, J.-J.; Kim, J. *Nanoscale Res. Lett.* **2009**, *4*, 364−370.
(11) Kuznetzov, A. A.; Lee, S. B.; Zhang, M.; Baughman, R. H.; Zakhidov, A. A. *Carbon* **2010**, *48*, 41−46.
(12) Fujii, S.; Honda, S.-I.; Kawai, H.; Ishida, K.; Oura, K.; Katayama, M. *Diam. Relat. Mater.* **2008**, *17*, 556−558.
(13) Nilsson, L.; Groening, O.; Emmenegger, C.; Kuettel, O.; Schaller, E.; Schlapbach, L.; Kind, H.; Bonard, J.-M.; Kern, K. *Appl. Phys. Lett.* **2000**, *76*, 2071−2073.
(14) Kong, Y. C.; Yu, D. P.; Zhang, B.; Fang, W.; Feng, S. Q. *Appl. Phys. Lett.* **2001**, *78*, 407−409.
(15) Wang, L.; Giles, N. C. *J. Appl. Phys.* **2003**, *94*, 973−978.
(16) Chang, Y.-M.; Shieh, J.; Chu, P.-Y.; Lee, H.-Y.; Lin, C.-M.; Juang, J.-Y. *ACS Appl. Mater. Interfaces* **2011**, *3*, 4415−4419.
(17) Fonoberov, V. A.; Balandin, A. A. *Appl. Phys. Lett.* **2004**, *85*, 5971−5973.
(18) Fonoberov, V. A.; Balandin, A. A. *Phys. Rev. B* **2004**, *70*, 195410−1-5.
(19) Fonoberov, V. A.; Balandin, A. A. *J. Phys: Condens. Matter.* **2005**, *17*, 1085−1097.
(20) Greene, L. E.; Law, M.; Goldberger, J.; Kim, F.; Johnson, J. C.; Zhang, Y.; Saykally, R. J.; Yang, P. *Angew. Chem., Int. Ed.* **2003**, *42*, 3031−3034.

(21) Kang, H. S.; Kang, J. S.; Kim, J. W.; Lee, S. Y. *J. Appl. Phys.* **2004**, *95*, 1246−1250.
(22) Li, D.; Leung, Y. H.; Djurišic, A. B.; Liu, Z. T.; Xie, M. H.; Shi, S. L.; Xu, S. J.; Chan, W. K. *Appl. Phys. lett.* **2004**, *85*, 1601−1603.
(23) Lin, B.; Fu, Z.; Jia, Y. *Appl. Phys. Lett.* **2001**, *79*, 943−945.
(24) Meng, X. Q.; Shen, D. Z.; Zhang, J. Y.; Zhao, D. X.; Lu, Y. M.; Dong, L.; Zhang, Z. Z.; Liu, Y. C.; Fan, X. W. *Solid State Commun.* **2005**, *135*, 179−182.
(25) Chang, Y.-M.; Jian, S.-R.; Lee, H.-Y.; Lin, C.-M.; Juang, J.-Y. *Nanotechnology* **2010**, *21*, 385705−1-7.
(26) Cai, P. F.; You, J. B.; Zhang, X. W.; Dong, J. J.; Yang, X. L.; Yin, Z. G.; Chen, N. F. *J. Appl. Phys.* **2009**, *105*, 083713−1-6.
(27) Tam, K. H.; Cheung, C. K.; Leung, Y. H.; Djurišic, A. B.; Ling, C. C.; Beling, C. D.; Fung, S.; Kwok, W. M.; Chan, W. K.; Phillips, D. L.; Ding, L.; Ge, W. K. *J. Phys. Chem. B* **2006**, *110*, 20865−20871.
(28) Fonoberov, V. A.; Alim, K. A.; Balandin, A. A. *Phys. Rev. B* **2006**, *73*, 165317−1-9.
(29) Fonoberov, V. A.; Balandin, A. A. *J. Nanoelectron. Optoelectron.* **2006**, *1*, 19−38.
(30) Xiu, F.; Yang, Z.; Zhao, D.; Liu, J.; Alim, K. A.; Balandin, A. A.; Itkis, M. E.; Haddon, R. C. *J. Cryst. Growth* **2006**, *286*, 61−65.
(31) Wang, X.; Zhou, J.; Lao, C.; Song, J.; Xu, N.; Wang, Z. L. *Adv. Mater.* **2007**, *19*, 1627−1631.
(32) Kumar, R. T. R.; McGlynn, E.; McLoughlin, C.; Chakrabarti, S.; Smith, R. C.; Carey, J. D.; Mosnier, J. P.; Henry, M. O. *Nanotechnology* **2007**, *18*, 215704−1-6.
(33) Cao, B.; Teng, X.; Heo, S. H.; Li, Y.; Cho, S. O.; Li, G.; Cai, W. *J. Phys. Chem. C* **2007**, *111*, 2470−2476.
(34) Marathe, S. K.; Koinkar, P. M.; Ashtaputre, S. S.; More, M. A.; Gosavi, S. W.; Joag, D. S.; Kulkarni, S. K. *Nanotechnology* **2006**, *17*, 1932−1936.
(35) Tzeng, Y.-F.; Wu, H.-C.; Sheng, P.-S.; Tai, N.-H.; Chiu, H. T.; Lee, C. Y.; Lin, I.-N. *ACS Appl. Mater. Interfaces* **2010**, *2*, 331−334.
(36) Ye, C.; Bando, Y.; Fang, X.; Shen, G.; Golberg, D. *J. Phys. Chem. C* **2007**, *111*, 12673−12676.
(37) Schlesser, R.; McClure, M. T.; McCarson, B. L.; Sitar, Z. *J. Appl. Phys.* **1997**, *82*, 5763−5772.
(38) Li, C.; Fang, G.; Liu, N.; Li, J.; Liao, L.; Su, F.; Li, G.; Wu, X.; Zhao, X. *J. Phys. Chem. C* **2007**, *111*, 12566−12571.
(39) Zhao, Q.; Zhang, H. Z.; Zhu, Y. W.; Feng, S. Q.; Sun, X. C.; Xu, J.; Yu, D. P. *Appl. Phys. Lett.* **2005**, *86*, 203115−1-3.
(40) Utsumi, T. *IEEE Trans. Electron Devices* **1991**, *38*, 2276−2283.
(41) Milne, W. I.; Teo, K. B. K.; Amaratunga, G. A. J.; Legagneux, P.; Gangloff, L.; Schnell, J.-P.; Semet, V.; Binh, V. T.; Groening, O. *J. Mater. Chem.* **2004**, *14*, 1−12.
(42) S. O. Kasap, *Principles of Electronic Materials and Devices*, 2nd ed., McGraw-Hill: New York, 2002; p 334.
(43) Aranovich, J. A.; Golmayo, D.; Fahrenbruch, A. L.; Bube, R. H. *J. Appl. Phys.* **1980**, *51*, 4260−4268.
(44) Lide, D. R.*CRC Handbook on Chemistry and Physics*; CRC Press: Boca Raton, FL, 2008; p12.